MULTI-SCALE SIMULATIONS OF LARGE SCALE FIBER BRIDGING IN MODE I INTRA-PLY FRACTURE

Luis P. Canal, Georgios Pappas, John Botsis

Laboratoire de mécanique appliquée et d'analyse de fiabilité, Ecole Polytechnique Fédérale de Lausanne (EPFL), CH-1015 Lausanne, Switzerland
Email: luis.canal@epfl.ch, Web Page: http://lmaf.epfl.ch

Keywords: Fracture of composites, Fiber bridging, Multiscale modelling, Fiber reinforced composites, Carbon fiber

Abstract
Multi-scale simulation strategies have demonstrated their ability to perform virtual tests of composite materials. These simulations strategies have an extraordinary interest due to the complexity of the failure mechanisms and the hierarchical microstructure in the case of fiber reinforced composites. In this work, an embedded cell simulation approach was used to study the toughening due to bridging in a unidirectionally reinforced carbon/epoxy composite in mode I intralaminar fracture. The numerical model was based on experimental information of the bridging mechanisms obtained from double cantilever beam experiments and microscopic observations of the bridging region. The actual microstructure of the bridging fiber bundles was represented along the mid-plane of the sample, while the rest of the specimen was simulated as an homogeneous solid. Numerical simulations were able to predict the initiation and propagation of failure as well as the development of bridging. The numerical model reproduced the thickness dependency experimentally observed.

1. Introduction

Fiber bridging is one of the most studied toughening mechanisms in composite materials [1, 2]. The mode I fracture of fiber reinforced composites (FRP) is usually acoompained by the development of numerous bridging ligaments that provide resistance to the crack propagation. In these materials, the extension of the bridging region is often comparable to the total crack length, resulting in a very noticeable increase of the fracture energy. This phenomenon is called Large Scale Bridging (LSB) and is experimentally observed in mode I fracture tests in Double Cantilever Beam (DCB) specimens. The results of these tests provide the resistance curves (R-curves), which show the increase of the fracture energy during crack propagation, as a direct consequence of the bridging development. However, recent experimental and numerical studies have shown that the R-curves obtained with mode I DCB tests in FRP is dependent on the specimen's geometry and should not be considered a material property [3, 4]. Manshadi et al. [5] and Framand-Ashtiani et al. [6] incorporated fiber Bragg grating sensors in the DCB specimens to measure the strains during mode I delamination and later identify an adequate cohesive law. These studies showed that the bridging zone length was linearly dependent with the thickness of the specimen. Similar behavior was observed by Pappas and Botsis [7] on mode I intralaminar fracture.

In this work, a multiscale simulation strategy based on an embedded cell model of the DCB test is employed to study the bridging mechanisms and the thickness dependency experimentally observed. The "virtual tests" provides important information about the influence of the constituents' properties in

Excerpt from ISBN 978-3-00-053387-7

the overall behavior of the composite material.

2. Materials and experiments

Unidirectional composite laminates were prepared by stacking 50 layers of carbon/epoxy pre-impregnate SE-70 (Gurit). The composite panel was consolidated in the autoclave at 78 °C and 3 bar pressure during 12 hours. DCB specimens were prepared by machining beams of 340mm long and 10 × H mm^2 cross sections. Three different thicknesses were considered H= 6, 10 and 14 mm. An initial precrack of 60mm was introduced in each specimen using a diamond wire and cubic loading blocks were bonded.

Mode I DCB tests were carried out according to the ASTM standard D5528 [8]. A constant cross-head opening of 3mm/min was applied using an Instron 5848 electromechanical testing machine and the force was simultaneously measured with a 2kN load cell. Furthermore, the evolution of the crack tip was recorded with a high resolution CCD camera during the test. The force-displacement curves obtained for the different thicknesses are shown in Figure 1 together with the R-curves (calculated with the modified compliance calibration method [8]). It is important to notice that the R-curves reached a plateau, which corresponds to the steady state of the crack propagation , and the level of this plateau was dependent on the specimen thickness.

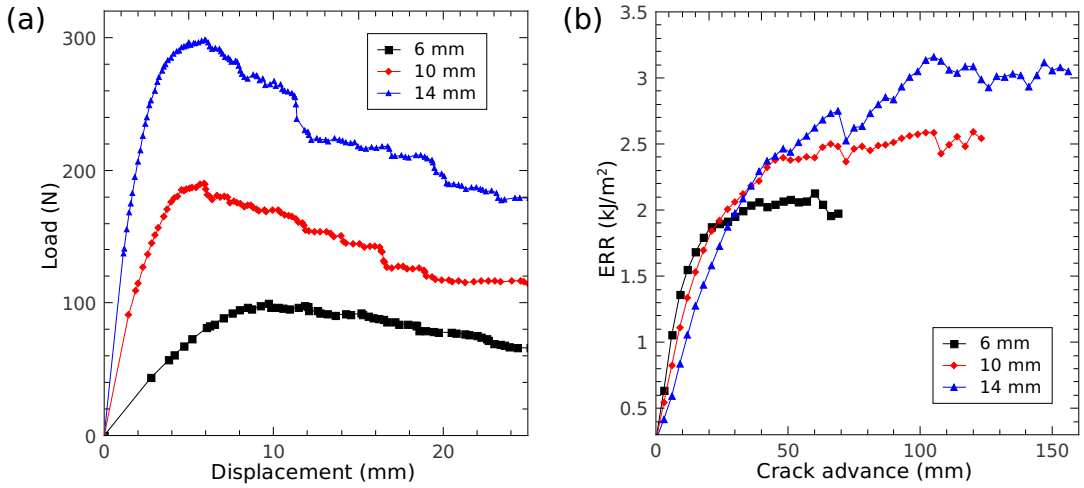

Figure 1. Experimental (a) Load-displacement and (b) resistance averaged curves obtained from mode I intralaminar DCB specimens with three different thickness.

3. Computational model

The model to simulate the mode I intralaminar fracture experiments consisted of an embedded cell model of the DCB specimen, following a strategy similar to the ones employed in [9–11]. The DCB specimen was represented by a three-dimensional model where the composite material was assumed homogeneous and anisotropic. This part was automatically meshed using 8-node linear brick elements (C3D8 in Abaqus [12]). The bridging bundles were explicity taken into account in the mid-plane of the specimen with 2-nodes linear beam elements (B31) with circular cross-section. The composite material in the homogeneous parts and in the bridging bundles was assumed an homogeneous and anisotrospic solid. The elastic properties were taken from [7] and are: E_x=118.7GPa, E_y=E_z=7.7GPa, G_{xy}=G_{xz}=3.8GPa, G_{yz}=3.1GPa, ν_{xy}=ν_{xz}=0.314 and ν_{yz}=0.427.

The bridging bundles were linked to the homogeneous parts with connector elements. The debonding

Excerpt from ISBN 978-3-00-053387-7

of the bridging bundles was taken into account with a linear force-opening softening law included in the connectors' behavior. The initial response was linear and elastic until it reached the maximum force and the subsequent onset of damage. This force-displacement law was reformulated into a stress-opening law considering the area affected by the connectors (Fig.2). The initial stiffness of the connectors was $K=10^8$ GPa/m. Two sets of properties were considered for the failure; weak connectors had a streght in tension of N_{weak}=40MPa and a failure energy of G_{weak}=300J/m^2. The two parameters for the strong connectors were $G_{strong}=1.5\times G_{weak}$ and $N_{strong}=1.5\times N_{weak}$. A random distribution of strong and weak connectors along the specimen was considered to trigger the bridging between the two sides of the DCB. Finally, a linear stress-strain degradation of the elastic properties was included in the material behavior of the bridging bundles through a User Defined Subroutine (USDFLD). The maximum stress controlling the onset of failure of the bundles was σ_{max} = 2000 MPa. Additional details about the model implementation can be found in [13].

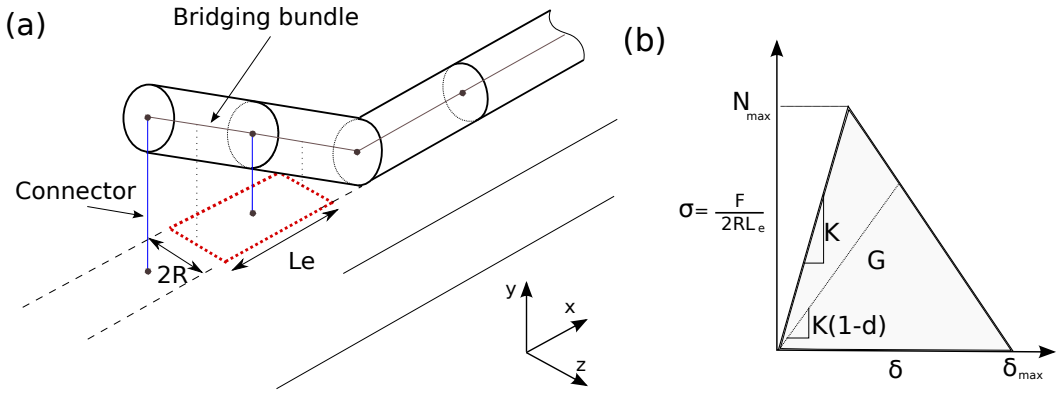

Figure 2. Schematic of (a) bridging bundle connected to the DCB specimen and (b) traction-separation law governing the behavior of the connectors.

4. Results and discussion

The simulation of the mode I DCB test was able to reproduce the micromechanisms experimentally observed. The intralaminar fracture appeared when some connectors ahead the pre-crack reached their maximum strength and failed. The propagation of the crack along the mid-plane of the specimen developed bridging bundles linking upper and bottom parts of the DCB specimen. The opening of the crack made the bridging bundles rotate and elongate resulting in a toughening mechanism similar to the one observed in the experiments (Fig.3).

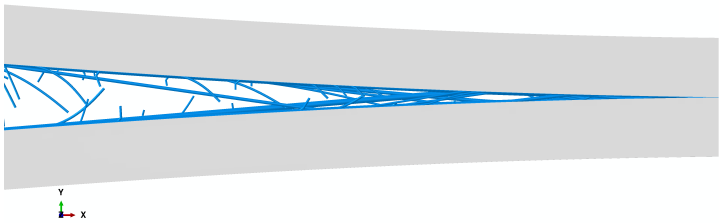

Figure 3. Detail of the bridging region obtained from the simulation of the DBC tests.

In addition to the bridging micromechanisms, the numerical model was able to reproduce the mechanical response of the DCB experiments. The force-displacement curves (Fig.4) provided by the numerical model showed an initial lineal and elastic loading before the crack initiated, higher loads produced a pro-

Excerpt from ISBN 978-3-00-053387-7

gressive degradation in the stiffness, until reaching a peak of maximum load. Further openings resulted in a decay of the load, reproducing the behavior experimentally observed. The three thicknesses studied showed different initial stiffness and maximum loads of ≈ 110, 220 and 360 N were achieved for the specimens of 6, 10 and 14 mm thick, respectively.

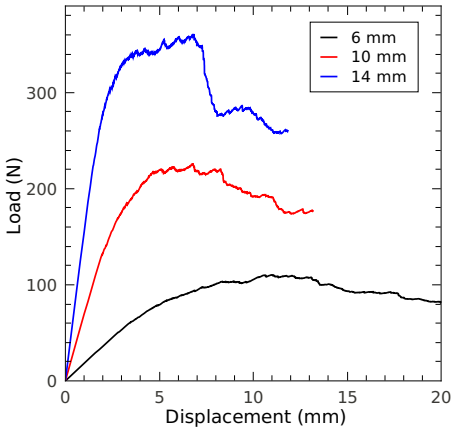

Figure 4. Force-displacement curves obtained from mode I intralaminar DCB simulation with three different thicknesses.

The force-displacement information, together with the crack tip position, allowed the determination of the R-curve by means of the modified compliance calibration method [8]. The Energy Release Rate (ERR) increased during the initial stages of the crack propagation as a direct consequence of the development of bridging Fig. 5. A plateau in the ERR was attained was attained when the bridging region was fully developed. The different thicknesses lead to different values of the plateau level, in good agreement with the experimental results. The thicker the specimen, the higher the ERR plateau in the simulation of the DCB test.

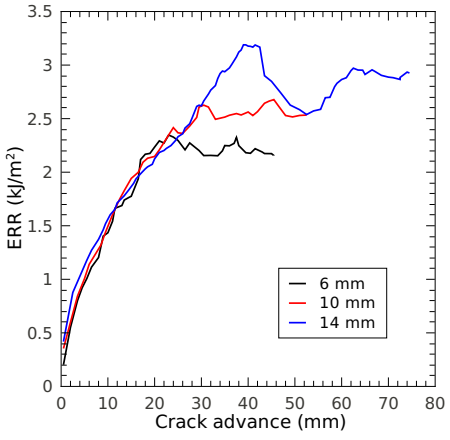

Figure 5. R-curves obtained from mode I intralaminar DCB simulation with three different thicknesses.

Excerpt from ISBN 978-3-00-053387-7

5. Conclusion

DCB mode I intralaminar fracture tests were simulated by means of an embedded cell model which takes into account the bridging developed during crack propagation. The numerical model was able to reproduce the toughening mechanisms experimentally observed. The force-displacement curves and the information about the crack tip position were employed to obtain the R-curves. The numerical model showed a thickness dependency on the energy released during crack propagation in good agreement with the experimental observations.

References

[1] B. F Sørensen and T. K Jacobsen. Large-scale bridging in composites: R-curves and bridging laws. *Composites Part A: Applied Science and Manufacturing*, 29:1443–1451, November 1998.

[2] L. Sorensen, J. Botsis, Th. Gmür and L. Humbert. Bridging tractions in mode I delamination: Measurements and simulations. *Composites Science and Technology*, 68:2350–2358, September 2008.

[3] G. Bao and Z. Suo. Remarks on Crack-Bridging Concepts. *Applied Mechanics Reviews*, 45:355–366, August 1992.

[4] Z. Suo, G. Bao, and B. Fan. Delamination R-curve phenomena due to damage. *Journal of the Mechanics and Physics of Solids*, 40:1–16, January 1992.

[5] B. D. Manshadi, E. Farmand-Ashtiani, J. Botsis, and A. P. Vassilopoulos. An iterative analytical/experimental study of bridging in delamination of the double cantilever beam specimen. *Composites Part A: Applied Science and Manufacturing*, 61:43–50, June 2014.

[6] E. Farmand-Ashtiani, J. Cugnoni, and J. Botsis. Specimen thickness dependence of large scale fiber bridging in mode I interlaminar fracture of carbon epoxy composite. *International Journal of Solids and Structures*, 55:58–65, March 2015.

[7] G. Pappas and J. Botsis. Intralaminar fracture of unidirectional carbon/epoxy composite: experimental results and numerical analysis. *International Journal of Solids and Structures*, 85-86:114-124, May 2016.

[8] ASTM D5528-13 Standard test method for mode I interlaminar fracture toughness of unidirectional fiber-reinforced polymer matrix composites.

[9] C. González, J. LLorca, Multiscale modeling of fracture in fiber-reinforced composites, Acta Materialia 54 (2006) 4171–4181.

[10] V. Šmilauer, C. G. Hoover, Z. P. Bažant, F. C. Caner, A. M. Waas and K. W. Shahwan. Multiscale simulation of fracture of braided composites via repetitive unit cells. *Engineering Fracture Mechanics*, 78:901–918, April 2011.

[11] L. P. Canal, C. González, J. Segurado and J. LLorca. Intraply fracture of fiber-reinforced composites: Microscopic mechanisms and modeling. *Composites Science and Technology*, 72:1223–1232, June 2012.

[12] *Abaqus, Users Manual, Version 6.121. Simulia.*

[13] L. P. Canal, G. Pappas, and J. Botsis. Large scale fiber bridging in mode I intralaminar fracture. An embedded cell approach. *Composites Science and Technology*, 126:52–59, April 2016.

Excerpt from ISBN 978-3-00-053387-7